Published in final edited form as:
J Am Chem Soc. 2013 October 9; 135(40): 14944–14947. doi:10.1021/ja408135g.

Intraduplex DNA-mediated electrochemistry of covalently tethered redox-active reporters

Catrina G. Pheeney and **Jacqueline K. Barton***

*Division of Chemistry and Chemical Engineering, California Institute of Technology, Pasadena, California 91125, USA

Abstract

Intraduplex DNA-mediated reduction is established as a general mechanism for the reduction of distally bound stacked redox-active species covalently tethered to DNA through flexible alkane linkages. Methylene Blue (MB), Nile Blue (NB), and Anthraquinone (AQ) were covalently tethered to DNA with three different covalent linkages. Using these reporters DNA electrochemistry was shown to be both DNA-mediated and intra-, rather than inter-, duplex. Significantly, the charge transport pathway occurring through the DNA π-stack is established by using an intervening AC mismatch to break this path. The fact that the DNA-mediated reduction of MB occurs primarily via intraduplex intercalation is established through varying the proximity and integrity of the neighboring duplex DNA.

DNA-modified electrodes are extensively used in both the development of next generation diagnostic sensors (1–6) and the characterization of ground-state DNA-mediated electrochemistry (7–15). Many different electrochemical reporters have been developed for DNA-modified electrodes, including: DNA-binding compounds (1, 5), quantum dots (4), and metallization (15, 16). Two classes of DNA-based devices have since emerged using the same covalently tethered intercalative compounds but different mechanisms: DNA conformation (3, 17–22) and DNA-mediated charge transfer (DNA CT) (6–14).

The DNA-mediated reduction of both freely diffusing and covalently tethered redox-active reporters has long been established on these DNA-modified electrodes (23–25). The strategy of covalently tethering redox-active reporters to the DNA, as opposed to the use of freely diffusing reporters, has been adopted to significantly diminish non-specific signals (11, 17). Redox-active reporters covalently tethered to DNA have been shown to electronically couple to the π-stack by a variety of mechanisms: end capping (13), intercalation (11, 12), and direct conjugation (14). However, the recent characterization of covalently tethered Methylene Blue (MB), an extensively used reporter for DNA-conformation based assays, has spurred a new debate with regards to the mechanism of its reduction (12, 19–21).

The capacity of these redox reporters to be reduced via an intraduplex DNA-mediated pathway has been brought into question with alternative mechanisms such as the duplex tilting to the surface, the charge traveling along the counter ions associated with the sugar phosphate backbone, or the reporter intercalating in a neighboring duplex (19–21). Here we

Corresponding Author. jkbarton@caltech.edu.

ASSOCIATED CONTENT

Supporting Information

Experimental procedures and supporting figures. This material is available free of charge via the Internet at http://pubs.acs.org.

Notes

The authors declare no competing financial interests.

demonstrate the generality of DNA-mediated reduction of covalently tethered reporters by varying both the redox-active species and the covalent linkage. Critical to these assays is the use of an intervening AC mismatch to establish that the charge transport pathway is through the duplex base pair stack. Beyond demonstrating that the reduction is DNA-mediated, we also provide evidence supporting an intraduplex process by varying the identity and proximity of neighboring duplex DNA.

The electronic coupling of redox-active reporters that are covalently tethered through a long (dT-C12-DNA) flexible alkane linkage was explored by linking three different NHS-ester activated redox reporters (MB, Nile Blue (NB), and Anthraquinone (AQ)) to the same amine-modified DNA (Figure 1). The reporter-modified DNA was annealed to a thiol-modified complement prior to the self-assembly on gold electrodes. Consistency between electrodes was ensured through the use of multiplexed chips containing 16 individually addressable electrodes (SI) (6). The midpoint potentials of the signals generated from densely packed DNA monolayers (assembled at 25 μM in the presence of 100 mM $MgCl_2$) labeled with MB, NB, and AQ are −300 mV, −420 mV, and −500 mV, respectively (Figure 1). Interestingly, the oxidative signal sizes are 6.1 ± 0.3 nC (MB), 2.8 ± 0.2 nC (NB), and 2.2 ± 0.4 nC (AQ), which is not consistent across the reporters. The signal sizes, however, correlate with the binding affinity of reporters based on their ability to thermally stabilize the duplex DNA (Supporting Table 2). Therefore, MB is well coupled to the π-stack compared to the relatively poorly coupled AQ. The quantity of immobilized DNA was determined using the electrostatic binding of $Ru(NH_3)_6^{3+}$ at low but saturating conditions based on titration (1 μM in 5.0 mM phosphate, 50 mM NaCl, pH 7.0) (Figure S1). Regardless of the redox reporter, the electrodes all were found to have surface coverages within error of each other, 5.2 ± 0.3 pmol/cm^2, consistent with that previously reported based on reporter reduction (12). This ensures that differences in signal sizes are not due to differences in the quantity of immobilized DNA.

In addition to varying the redox-active species, both the length of the covalent linkage and the placement of the redox-active reporter were also probed (Figure 2). In addition to the long C12 linkage appended off the thymine, two new linkages were prepared: a shortened C8 linkage appended off the modified thymine in the same manner and a C12 linkage instead appended off the 5′ hydroxyl (26). Densely packed monolayers were compared for MB (Figure 2) and NB (Figure S2) covalently tethered to the DNA through these three linkages. Taken together, the midpoint potential, peak splitting, and signal size create a distinct reproducible profile for each linkage (Table S3). Notably, differences are observed in the signals generated from MB covalently tethered via the same C12 linkages appended to the thymine and 5′ hydroxyl as well as between both the short and long linkages appended off the thymine. These distinct electrochemical profiles indicate that both the placement and length of the covalent tether play critical roles in dictating the coupling of the reporter with the base pair stack and therefore the kinetics of the redox signal. For example, the difference in midpoint potential between the dT-C12 and dT-C8 linkages is attributed to the truncated linkage, decreasing the binding affinity of the reporter; in fact, the midpoint potential shift results solely from a shift in the reduction peak, while the oxidative peak remains relatively constant. This differential behavior of the reductive and oxidative peaks can be understood based on the lowered binding affinity of the reporter in the reduced form (27). The shift in the midpoint potential of the 5’ hydroxyl linkage is attributed to binding via an end-capping mode as opposed to intercalation (13). Additionally, based on poorer coupling, NB consistently shows a decreased signal size (40% – 80%) compared to MB for all three linkages under all conditions examined.

The degree of DNA-mediated reduction for this family of redox reporters and linkages was assessed by introducing a single mismatched base pair intervening between the redox

reporter and the gold electrode. This is an *essential* assay of DNA-mediation. DNA CT is known to be exquisitely sensitive to subtle perturbations to the π-stack; therefore the introduction of even a single intervening mismatched base pair (AC) significantly attenuates the overall yield of electrons reaching the distally bound reporter when the signals are generated via a DNA-mediated pathway (7, 24). This diminished yield of reporter reduction is seen to be associated with incorporation of a single base pair mismatch even in a 100-mer and over a wide range of temperatures (9, 28). Here direct comparisons between fully well-matched and AC mismatched 17-mer DNA were performed on the same multiplexed surface to reduce effects caused by the assembly conditions and surface quality. The percent signal remaining with a single AC mismatch was determined relative to well- matched DNA for all linkages and for both MB and NB (Table 1). Although AQ appended by a C12 linkage to the terminal thymine was also shown to display significant signal attenuation upon introducing a single AC mismatch (Figure S3), its negative midpoint potential and oxygen- mediated electrocatalytic activity made signal quantification challenging. Overall, AQ poses the most challenges to quantification and is poorly coupled to the π-stack so it was not further investigated as an electrochemical reporter for DNA CT.

The degree of signal attenuation upon mismatch incorporation was characterized under both low and high density conditions. It has previously been established that the DNA-mediated reduction of MB-dT-C12-DNA is exceptionally sensitive to the assembly conditions of the electrode, yielding a greater DNA-mediated signal upon decreased surface accessibility of the reporter (12). All linkages attaching both MB and NB displayed significant signal attenuation upon incorporation of a single AC mismatch under high density conditions, validating that the predominant mechanism for reduction is a DNA-mediated pathway (Figure 2 and Table 1). The quantity of immobilized DNA was again verified by the addition of $Ru(NH_3)_6^{3+}$ (1 μM). DNA surface coverages were found to be within error of one another for well-matched or mismatched DNA for both film densities, 5.2 ± 0.3 pmol/cm^2 and 3.0 ± 0.3 pmol/cm^2 for high and low density respectively (Figure 3 and S4). This ensured that the observed differences in signal were not a result of altered hybridization efficiency caused by the incorporation of the AC mismatch. Finally, the scan rate was varied from 50 mV to 13 V to establish the rate of electron transfer for MB with both dT-C8 and dT-C12 linkages (Figure S5). Based on the Laviron analysis they displayed similar rates of electron transfer (2–4 s^{-1}), consistent with previously established results for a DNA-mediated mechanism where tunneling through the alkane-thiol is rate limiting (8, 12).

Under low density conditions, the percent signal remaining upon incorporation of a single AC mismatch ranged from 60% – 90%, compared to the high density conditions where it ranged from 10% – 40% across both reporters and all linkages (Table 1). The general nature of this dependence on film density speaks to the validity of our proposed mechanism, where surface accessibility dictates whether or not charge transport proceeds via DNA-mediated or surface-mediated pathways. Additionally, this demonstrates the utility of the truncated dT-C8 linkage as a means of decreasing the surface accessibility of the reporter as it retains the most DNA-mediated character under low density conditions.

The proximity of the neighboring duplex DNA within the monolayer was again varied, this time including the additional assembly condition of 1 mM $MgCl_2$, to provide further support that DNA-mediated reduction is favored under conditions of high surface coverages and not simply because of the addition of $MgCl_2$ during assembly. The addition of $MgCl_2$ during monolayer formation has been used for over a decade to control the density of DNA monolayer packing (2, 7). As previously mentioned, 100 mM $MgCl_2$ has been used to produce dense DNA monolayers that physically extrude the reporter from directly accessing the electrode surface therefore enhancing DNA-mediated electrochemistry; however, it has

yet to be determined whether this effect results from simply the addition of $MgCl_2$ during assembly or from the increased surface coverages obtained at high $MgCl_2$ concentrations.

Signal attenuation upon introducing a single AC mismatch and the concentration of immobilized DNA, based on the electrostatic binding of $Ru(NH_3)_6^{3+}$, were quantified for MB covalently tethered by both dT-C8 and dT-C12 linkages at three different DNA monolayer conditions, incubation without $MgCl_2$, with 1 mM $MgCl_2$, and with 100 mM $MgCl_2$ (Figure S7). The observed signal attenuation upon incorporation of an AC mismatch and the DNA surface coverage in the 1 mM MgCl2 film is not altered compared to signals for DNA monolayers assembled without $MgCl_2$ (Figure s7). As the sensitivity to π-stack perturbations is only enhanced at higher DNA surface coverages, this result further supports the model where the extent of the exposed electrode surface dictates the mechanism of either DNA-mediated or surface-mediated reduction.

The significance of the neighboring duplex integrity was investigated by introducing increasing fractions of unlabeled duplex DNA with a single AC mismatch. DNA-modified electrodes were assembled using a 50/50 mixture of well-matched MB-modified DNA and unlabeled DNA of varying compositions of well-matched and mismatched DNA. As the truncated dT-C8 linkage displays DNA-mediated character under both high and low density conditions it was used to establish whether inter- or intra- duplex intercalation is the predominant mode of reporter binding to the π-stack (Figure 4). Results for the dT-C12 linkage were included for completeness (Figure S6). As the fraction of well-matched MB-modified DNA remains constant, an attenuation of signal would only be expected in the presence of higher fractions of mismatched DNA if the reduction occurred through an interduplex pathway, as opposed to an intraduplex pathway where the signal is expected to remain unaltered. The predicted extent of signal attenuation for an interduplex pathway was calculated at each mismatch concentration based on the fraction of mismatched DNA in the film and the percent signal attenuation previously determined for a 100% mismatched DNA film for both assembly conditions (Table 1). In all cases, the experimental results of incorporating mismatched DNA showed significantly less signal attenuation than predicted, consistent with a predominantly intraduplex pathway (Figure 4). Most notably, for the case of the low density DNA films, the effect is less than 5% of that predicted, suggesting that 95% of the DNA-mediated signal is generated via an intraduplex pathway. Therefore, there is roughly 20-fold more intraduplex reduction occurring than interduplex reduction within these films. Even in the densely packed DNA monolayers where the decreased distance between duplexes would facilitate interduplex intercalation of the reporter, the observed attenuation was still only 25% of that predicted, indicating that intraduplex reduction is still 3-fold more favored than an interduplex pathway.

Thus, we have demonstrated that intraduplex DNA CT is the primary mechanism for the redox-activity of probe molecules that are covalently tethered to a DNA duplex and well stacked. The extent of DNA-mediated electronic coupling depends not only on how tightly the redox-active species interacts with the π-stack but also the location and structure of the covalent tether. Finally, the possibility by which charge transport occurs through the counter ions associated with the sugar-phosphate backbone or the reporter intercalating into the neighboring duplex are not supported by our results. Instead we observe reporter sensitivity to intervening π-stack perturbations and a tolerance to the integrity of the neighboring duplex DNA. These results fully support the intraduplex DNA-mediated reduction of these covalently tethered reporters. Ultimately, delineating the mechanisms of electron transfer in DNA-modified electrodes is critical for their continued development as useful diagnostic tools.

Supplementary Material

Refer to Web version on PubMed Central for supplementary material.

Acknowledgments

We are grateful for the support of NIH (GM61077). We also thank the Kavli Nanoscience Institute facilities and staff for help in fabricating the multiplexed chips.

REFERENCES

1. Lam B, Fang Z, Sargent EH, Kelley SO. Anal. Chem. 2012; 84:21. [PubMed: 22142422]
2. Lapierre MA, O'Keefe M, Taft BJ, Kelley SO. Anal Chem. 2003; 75:6327. [PubMed: 14616017]
3. Zhao S, Yang W, Lai RY. Biosens. Bioelectron. 2011; 26:2442. [PubMed: 21081271]
4. Kwon SJ, Bard AJ. J. Am. Chem. Soc. 2012; 134:10777. [PubMed: 22702801]
5. Pheeney CG, Guerra LF, Barton JK. Proc. Natl. Acad. Sci. 2012; 109:11528. [PubMed: 22733728]
6. Slinker JD, Muren NB, Gorodetsky AA, Barton JK. J. Am. Chem. Soc. 2010; 132:2769. [PubMed: 20131780]
7. Kelley SO, Jackson NM, Hill MG, Barton JK. Angew. Chem. Int. Ed. 1999; 38:941.
8. Drummond TG, Hill MG, Barton JK. J. Am. Chem. Soc. 2004; 126:15010. [PubMed: 15547981]
9. Slinker JD, Muren NB, Renfrew SE, Barton JK. Nat. Chem. 2011; 3:228. [PubMed: 21336329]
10. Pheeney CG, Arnold AR, Grodick MA, Barton JK. J. Am. Chem. Soc. 2013; 135:11869. [PubMed: 23899026]
11. Kelley SO, Barton JK, Jackson N, Hill MG. Bioconjugate Chem. 1997; 8:31.
12. Pheeney CG, Barton JK. Langmuir. 2012; 28:7063. [PubMed: 22512327]
13. Boon E, Jackson N, Wightman M, Kelley S, Hill M, Barton JK. J. Phys. Chem. B. 2003; 107:11805.
14. Gorodetsky A, Green O, Yavin E, Barton JK. Bioconjugate Chem. 2007; 18:1434.
15. Weizmann Y, Chenoweth DM, Swager TM. J. Am. Chem. Soc. 2011; 133:3228.
16. Wu J, Chumbimuni-Torres KY, Galik M, Thammakhet C, Haake DA, Wang J. Anal. Chem. 2009; 81:1007.
17. Plaxco KW, Soh HT. Trends Biotech. 2011; 29:1.
18. Bonham AJ, Hsieh K, Ferguson BS, Vallee-Belisle A, Ricci F, Soh HT, Plaxco KW. J. Am. Chem. Soc. 2012; 134:3346. [PubMed: 22313286]
19. Abi A, Ferapontova EE. J. Am. Chem. Soc. 2012; 134:14499. [PubMed: 22876831]
20. Farjami E, Campos R, Freapontova EE. Langmuir. 2012; 28:16218. [PubMed: 23106377]
21. Yu Z, Lai RY. Anal. Chem. 2013; 85:3340. [PubMed: 23413882]
22. Wu Y, Lai RY. Chem. Comm. 2013; 49:3422. [PubMed: 23503676]
23. Wagenknecht, HA., editor. Charge Transfer in DNA:From Mechanism to Application. Weiheim: Wiley-VCH; 2005.
24. Genereux JC, Barton JK. Chem. Rev. 2010; 110:1642. [PubMed: 20214403]
25. Murphy CJ, Arkin MR, Jenkins Y, Ghatlia ND, Bossmann SH, Turro NJ, Barton JK. Science. 1993; 262:1025. [PubMed: 7802858]
26. There is precedence for MB-modified DNA with all of the linkages used here: dT-C12 (12, 19), dT-C8 (5), and 5′-C12 (13, 20).
27. Boon EM, Barton JK, Bhaghat V, Nerissian M, Wang W, Hill MG. Langmuir. 2003; 19:9255.
28. Wohlgamuth CH, McWilliams MA, Slinker JD. Anal. Chem. 2013; 85:1462. [PubMed: 23252597]

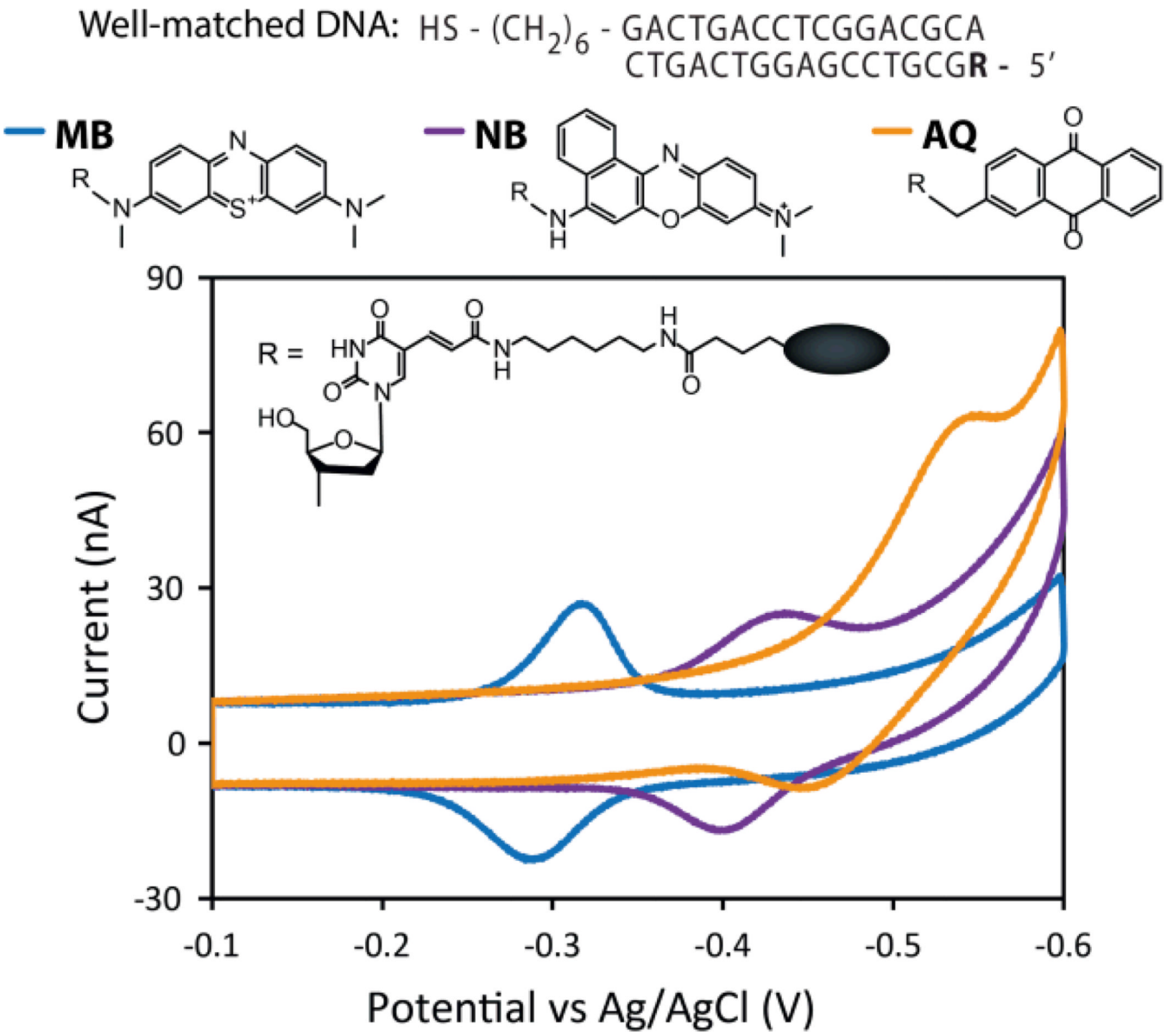

Figure 1.

Variation of redox-active species. Structures (top) and cyclic voltammetry (scan rate = 100 mV/s)(bottom) of MB (blue), NB (purple), and AQ (orange) modified DNA covalently tethered via a C12 flexible alkane linkage on a modified thymine. DNA-monolayers were assembled in the presence of 100 mM $MgCl_2$, backfilled with 6-mercaptohexanol (1 mM for 45 min), and scanned in spermidine buffer, see SI for full methods.

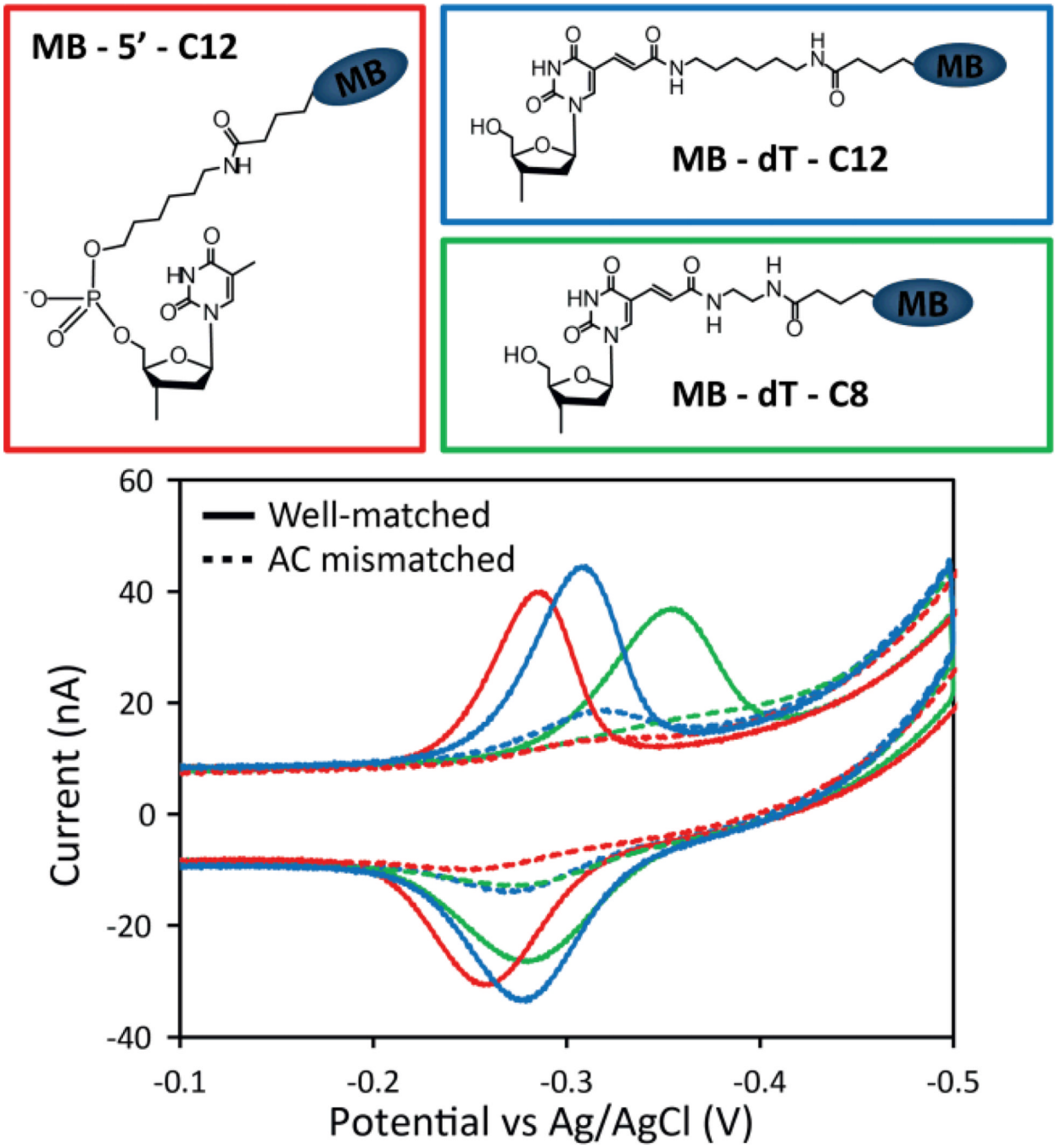

Figure 2.
Variation of covalent linkage. Structures (top) and cyclic voltammetry (scan rate = 100 mV/s) (bottom) of MB covalently tethered to duplex DNA via three different linkages: 5′-C12 (red), dT-C12 (blue), and dT-C8 (green). The signals from well-matched (solid) and AC mismatched (dashed) 17-mer DNA are both presented, sequences available in SI.

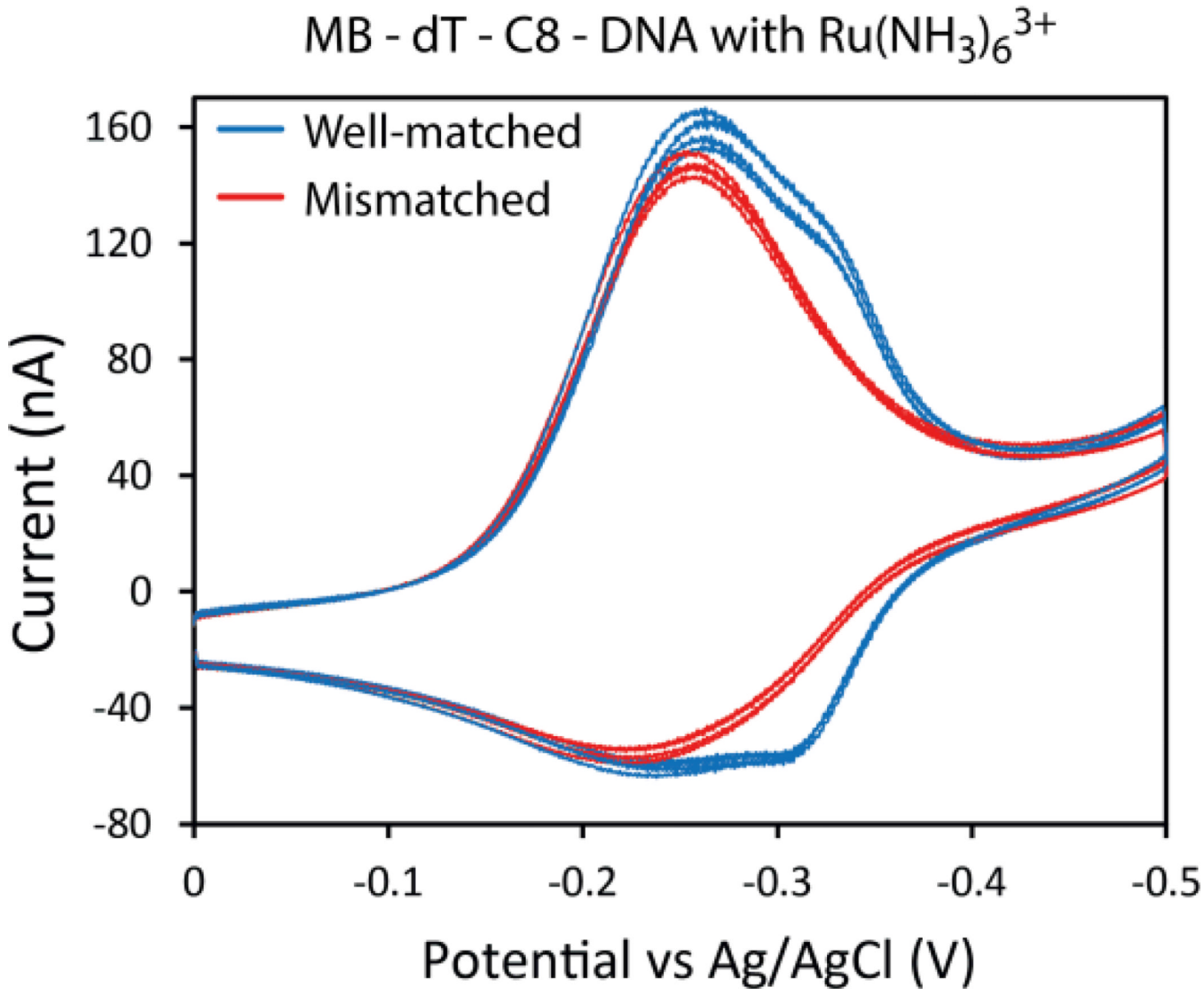

Figure 3.

Consistency of $Ru(NH_3)_6^{3+}$ quantification across DNA sequences in high density DNA monolayers. Representative cyclic voltammograms (scan rate = 100mV/s) of the quantification of immobilized DNA by the electrostatic binding of $Ru(NH_3)_6^{3+}$ (1 μM) in phosphate buffer are presented for MB-dT-C8-DNA. Well-matched (blue) and AC mismatched (red) 17-mer DNA are presented. 4 individual electrodes are presented to demonstrate the variability observed. Signals from both $Ru(NH_3)_6^{3+}$ and MB are present at −250 mV and −300 mV respectively. Only the MB signal shows significant signal attenuation upon mismatch incorporation.

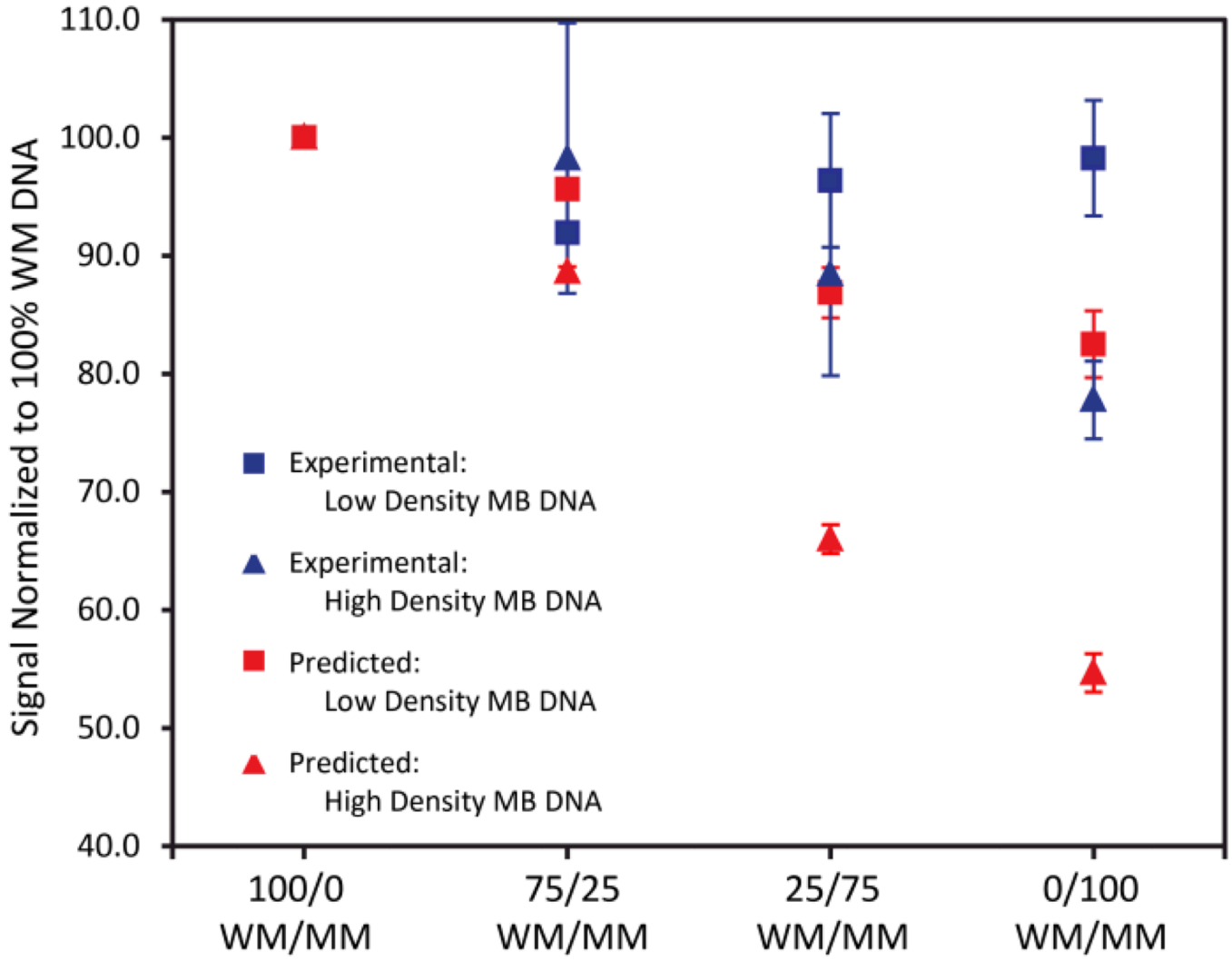

Figure 4.

Effect of neighboring duplex integrity for MB-dT-C8-DNA. Electrodes assembled with MB-modified well-matched DNA and varied fractions of unlabeled well-matched and AC mismatched DNA. The experimental (blue) reductive signal areas were determined at each fraction of unlabeled mismatched DNA and normalized to the signal at 100% well-matched DNA. The predicted values were determined by the total fraction of mismatched DNA times by the percent signal attenuation for the given linkage and assembly conditions. Electrodes assembled in the presence (triangle) and absence (square) of 100 mM $MgCl_2$ are presented.

Table 1

Percent signal remaining for MB and NB modified DNA for all covalent linkages examined in high and low density DNA monolayers.

Covalent Tether	Percent Signal Remaining (MM/WM*100) [b, c]	
	MB-DNA	NB-DNA
High Density		
dT-C_8	9	42
dT-C_{12}	18	N/A[a]
$^{5'}$-C_{12}	6	15
Low Density		
dT-C_8	65	66
dT-C_{12}	89	N/A[a]
$^{5'}$-C_{12}	61	75

[a] Data were not acquired due to low synthetic yields.

[b] Errors on all percent signal remaining are ± 1 %.

[c] WM is well-matched and MM is AC mismatched.